Theor Appl Climatol (2010) 99:331–344
DOI 10.1007/s00704-009-0142-9

ORIGINAL PAPER

A new building energy model coupled with an urban canopy parameterization for urban climate simulations—part I. formulation, verification, and sensitivity analysis of the model

Francisco Salamanca · Andrea Krpo · Alberto Martilli · Alain Clappier

Received: 21 October 2008 / Accepted: 21 April 2009 / Published online: 13 May 2009

Abstract The generation of heat in buildings, and the way this heat is exchanged with the exterior, plays an important role in urban climate. To analyze the impact on urban climate of a change in the urban structure, it is necessary to build and use a model capable of accounting for all the urban heat fluxes. In this contribution, a new building energy model (BEM) is developed and implemented in an urban canopy parameterization (UCP) for mesoscale models. The new model accounts for: the diffusion of heat through walls, roofs, and floors; natural ventilation; the radiation exchanged between indoor surfaces; the generation of heat due to occupants and equipments; and the consumption of energy due to air conditioning systems. The behavior of BEM is compared to other models used in the thermal analysis of buildings (CBS-MASS, BLAST, and TARP) and with another box-building model. Eventually, a sensitivity analysis of different parameters, as well as a study of the impact of BEM on the UCP is carried out. The validations indicate that BEM provides good estimates of the physical behavior of buildings and it is a step towards a modeling tool that can be an important support to urban planners.

F. Salamanca (✉) · A. Martilli
Department of Environment, CIEMAT
(Center for Research on Energy, Environment and Technology),
Edificio 3, P1.9, Avenida Complutense 22,
28040 Madrid, Spain
e-mail: francisco.salamanca@ciemat.es

A. Krpo · A. Clappier
LPAS, Swiss Federal Institute of Technology,
Lausanne, Switzerland

1 Introduction

In the last decades, atmospheric scientists have been able to understand the origin of the temperature differences between an urban area and its surroundings, the so-called urban heat island (UHI) (Oke 1987). This understanding has been possible thanks to a series of experimental campaigns, to the evolution of the mesoscale meteorological models, and the increase of computer power. In the 1970s and 1980s, scientists began to introduce urban parameterizations in numerical mesoscale models to determine how cities affect the meteorological fields and the boundary layer structure. However, these first parameterizations were still very simple and could not reproduce in detail the dynamics of the interactions between a city and the atmosphere. It is only during the second part of the 1990s and the beginning of the twenty-first century that more realistic urban parameterizations appeared (Masson 2000; Kusaka et al. 2001; Martilli et al. 2002).

The models developed in this period allowed to better understand the phenomena linked to the atmosphere over cities and their surroundings. However, the generation of heat within buildings and the exchanges with the exterior were not explicitly resolved. One of the first models that took these features into account was the one developed by Kikegawa et al. (2003). It was successfully implemented in an urban canopy parameterization (UCP) for mesoscale models and clearly showed that the heat fluxes generated by building can have an important impact on the urban microclimate.

In this contribution, a new building energy model (BEM) has been worked up and implemented in an UCP for mesoscale models. It is important to remark that, due to computational requirements, we cannot take into account

all the details in the interactions between buildings and the atmosphere. In fact, reducing complexity is particularly important as the final goal is to link BEM with a mesoscale meteorological model. Moreover, the current computing capacity does not allow resolving each specific building included in a grid cell of the meteorological model, usually of the order of a few squared kilometers. Even though all buildings are different, it is necessary to develop a model that describes the general physical properties of an ideal building, representative of the buildings included within the grid cell, as the purpose is to investigate the interactions between urban climate, air pollution, and energy consumption at the scale of the city and its surroundings. On the other hand, a very simple BEM would not be capable of describing accurately the most important interactions between buildings and the atmosphere, and would not be sufficient to study the interactions mentioned above, when implemented in a mesoscale model.

For these reasons, in this work we propose a new model that resolves explicitly:

- the heat diffusion through walls, roofs and floors
- the natural ventilation as well as the radiation exchanged between the indoor surfaces
- the heat generation due to occupants and equipments
- the energy consumption due to air conditioning systems

Buildings of several floors can be considered and the time evolution of indoor air temperature and moisture are estimated for each floor. Different floors can receive different amounts of radiation and can have different temperatures, both outdoor (e. g. for skyscrapers) and indoor. It is logical to think that the cooling/heating loads (energy consumption) will also be different at each level.

The links between BEM and UCP are as follows: UCP gives to BEM the outdoor air temperature, humidity, and radiation reaching the walls and roof for the computation of the amount of radiation entering in the building through the windows and the boundary condition for the calculation of wall and roof temperatures; on the other hand, BEM gives to the UCP the wall and roof temperature, the heat flux due to ventilation, and the heat flux due to processes linked with the generation of energy within the building (e. g. air conditioning). The expected results of this study are:

- To improve the capability of mesoscale models to simulate urban canopy climate (UHI processes, etc.) and air pollutant dispersion in the city and the surroundings
- To allow the estimation of meteorologically related building energy consumptions (e. g. due to air conditioning in summer, or heating in winter)

In Section 2 the model formulation is described. In Section 3, we validate BEM comparing it to well-known models like CBS-MASS, BLAST, and TARP for three different situations (Zmeureanu et al. 1987). The total processed loads obtained with BEM and Kikegawa´s model in a 25-story office building are also compared. In Section 4, after this necessary validation, we analyze numerical results by modifying some physical parameters to evaluate their impact on the processed load. In Section 5, first results about the impact of BEM in the UCP of Martilli et al. (2002) are shown and conclusions are finally given in Section 6. In part II of this work, BEM coupled with the UCP is validated against meteorological measurements from the BUBBLE campaign (Salamanca and Martilli 2009).

2 Description of BEM

The model used here is similar to that of Kikegawa et al. (2003). In Kikegawa´s model, a building is treated as a box and the generated cooling/heating loads are separately calculated for sensible and latent heat components. The heat pumped out from the building is "proportional" to this load (more details in Section 2.5). The main differences between the two models are the computation of the solar radiation reaching the indoor walls, the treatment of the windows, the computation of the heat pumped out from the building for cooling or added for heating, and the possibility to consider several floors in a building. The BEM developed in this paper is a box-type heat budget model in which a building in an urban block is treated as a pile of boxes, each box representing a particular floor.

2.1 Dynamics and thermodynamics

In BEM, the time evolutions of the room air temperature T_r and room air humidity q_{Vr} are estimated solving the following equations:

$$Q_B \frac{dT_r}{dt} = H_{in} - H_{out} \quad (1)$$

$$l\rho V_B \frac{dq_{Vr}}{dt} = E_{in} - E_{out} \quad (2)$$

in which $Q_B = \rho C_p V_B (JK^{-1})$ and $V_B(m^3)$ denote the overall heat capacity and the total volume of the indoor air in a floor (the reader can see more details about the symbols used in the previous and following equations in the Appendix). The following equations (Eqs. 3 and 4) were used for the computation of the total sensible heat load

$H_{in}(W)$ and the total latent heat load $E_{in}(W)$ in a floor, respectively:

$$H_{in} = \sum_j A_j^{wind} h_{wind,j}\left(T_{wind,j} - T_r\right) + \sum_i A_i^{wall} h_{wall,i}\left(T_{wall,i} - T_r\right) +$$

$$+(1-\beta)C_p \rho V_a (T_a - T_r) + A_f q_E + A_f P \phi_p q_{hs} \quad (3)$$

$$E_{in} = (1-\beta) l \rho V_a (q_{Va} - q_{Vr}) + A_f P \phi_p q_{hl} \quad (4)$$

The first and second term (on the right-hand side) in Eq. 3 represent the heat exchange between the windows and the indoor air and between the walls, ceiling, and pavement and the indoor air. The third term corresponds to the sensible heat exchange through ventilation. The fourth and the last terms indicate the internal sensible heat generation from equipments and occupants, respectively. The quantification of these last terms is difficult and it is necessary to have some information about the energy consumption provided by the electric companies. The heat from these different processes is added and distributed isotropically in the interior. A real diffusion through the indoor air is not considered in the model. The first right-hand term of Eq. 4 represents the water vapor mixing through ventilation and the second term the evaporation from occupants. The terms $H_{out}(W)$ and $E_{out}(W)$ indicate the sensible and latent heat needed for cooling/heating the indoor air in a floor. Remark that if there is no human regulation of the internal temperature and humidity these two terms are zero.

2.2 Computation of the wall temperature

In order to compute the wall temperature, the heat diffusion equation is solved in several layers at the interior of the materials. The transport of moisture through the walls is not considered,

$$\frac{\partial T_{wall}}{\partial t} = \frac{\partial}{\partial x}\left(K_s \frac{\partial T_{wall}}{\partial x}\right) \quad (5)$$

where K_s ($m^2\ s^{-1}$) is the thermal conductivity of the material, T_{wall} is the wall temperature. At the indoor and outdoor surfaces, the boundary condition is defined by solving an energy budget equation (neglecting the latent heat flux),

$$\frac{\partial T_{wall}}{\partial t} = \frac{1}{\Delta x}\left(C_s^{-1} HF - K_s \frac{\partial T_{wall}}{\partial x}\bigg|_{n-1}\right) \quad (6)$$

where $HF = (1-\text{alb})R_s + \varepsilon Rl - \varepsilon\sigma T_{wall}^4 + H$[1]. The term C_s ($J\ K^{-1}\ m^{-3}$) is the specific heat of the layer of depth Δx, and H ($W\ m^{-2}$) is the sensible heat flux exchanged between the surface and the air (a positive value means a gain for the surface). It is computed as $H = h_{wall}(T_r - T_{wall})$ in the indoor side and $H = h(T_r - T_{wall})$ in the outdoor side. The term R_s is the shortwave radiation flux incoming at the surface, Rl is the long-wave radiation received by the surface, and finally, alb and ε are the surface albedo and emissivity respectively. This budget equation is solved on both sides of the wall.

2.3 Computation of the window temperature

We suppose that the differences in temperature between the two sides of a glass are small, and, as a consequence, the temperature of the windows is only time-dependent. In order to compute the temperature of the glass of the window (T_{wind}), we suppose that the absorption is negligible (glasses without coating or films) and the following budget equation is solved:

$$C\frac{dT_{wind}}{dt} = \phi \quad (7)$$

where $C = \rho_{wind} C_{wind} \Delta_{wind}\left(JK^{-1}m^{-2}\right)$, ρ_{wind} ($kg\ m^{-3}$)is the density of the glass, C_{wind} ($JK^{-1}\ kg^{-1}$) is the heat capacity of the glass, Δ_{wind} (m) is the thickness of the glass, and $\phi\left(Wm^{-2}\right)$ is the total flux balance of energy,

$$\phi = \varepsilon_{wind}\left(Rl_{outdoor} - \sigma T_{wind}^4\right) + H_{outdoor} + \varepsilon_{wind}\left(Rl_{indoor} - \sigma T_{wind}^4\right) + H_{indoor} \quad (8)$$

The terms H_{indoor} and $H_{outdoor}$ are the sensible heat fluxes, while Rl_{indoor} and $Rl_{outdoor}$ are the incoming long-wave radiation on each side of the window. The windows are assumed opaque to the long-wave radiation.

2.4 Computation of the radiation

The amount of direct radiation that passes through a window is a function of the angle of incidence and will be computed with a polynomial approach based on Roos (1997) and used by Karlsson and Roos (2000) and others. The model employs a polynomial to fit the angle dependence of the total solar energy transmittance **g**, based upon the knowledge of the respective near-normal value g_0. The general form of the polynomial is $g(z) = g_0(1 - az^{\alpha} - bz^{\lambda} - cz^{\gamma})$, where $a+b+c=1$, $z = \theta^0/90^0$, and θ_0 is the angle of incidence. When fitting to different types of windows it was found that the above equation gives a good fit with the following coefficients and exponents:

$$\begin{aligned} &a = 8,\ b = 0.25/q,\ c = 1-a-b,\\ &\alpha = 5.2 + 0.7q,\ \lambda = 2,\\ &\gamma = 5.26 + 0.06p + (0.73 + 0.04p)q. \end{aligned} \quad (9)$$

In Eq. 9, p is equal to the number of panes in the configuration (1, 2, or 3) and q represents a 'category'

[1] To solve numerically the equation, the wall is discretized in several layers of depth Δx. Here and in Eq. 6 T_{wall} represents the temperature of the layer close to the surface, while $\frac{\partial T_{wall}}{\partial x}\big|_{n-1}$ represents the gradient between the layer close to the surface and the closest internal layer.

parameter, which has been given values between 1 and 10 depending on the type of window (q=4, for standard glasses).

The computation of the diffused and reflected radiation that passes through a window can be calculated using the albedo of that window (alb_{wind}). The albedo of a window can be evaluated (suppose that the absorption is negligible) equalizing the energy that crosses the glass with ($1-\text{alb}_{\text{wind}}$) times the energy that reaches the window. Writing this in mathematical form, see Fig. 1, we can say

$$\left(\int_0^{2\pi}\int_0^{\frac{\pi}{2}} g(\theta) I\cos\theta dw\right) dA = (1-\text{alb}_{\text{wind}}) F dA \qquad (10)$$

where I is the intensity of the radiation and F is the flux of energy reaching the element of surface dA (it is obtained integrating the intensity over all the possible directions). Considering isotropy (I constant) and simplifying by the differential area dA, the above expression becomes,

$$2\int_0^{\frac{\pi}{2}} g(\theta)\cos\theta\sin\theta d\theta = (1-\text{alb}_{\text{wind}}) \qquad (11)$$

With a simple algebraic manipulation, the albedo of the window can be written as

$$\text{alb}_{\text{wind}} = 1 - g_0 + \frac{g_0}{2}\int_0^{\pi}\left(\frac{a}{\pi^{\alpha}}x^{\alpha} + \frac{b}{\pi^{\lambda}}x^{\lambda} + \frac{c}{\pi^{\gamma}}x^{\gamma}\right)\sin x dx \qquad (12)$$

We now have a simple expression (Eq. 12) that depends only on two parameters (p, q) to evaluate the quantity of radiation transmitted through the windows when the radiation is not direct. Using a numerical method it is easy to evaluate this expression. In the simulations presented in this work, we have used Eq. 12 to evaluate all the shortwave radiation that penetrates the windows. Once the module is linked to the UCP, this formulation is used for the direct and reflected radiation from the other surfaces of the urban canyons.

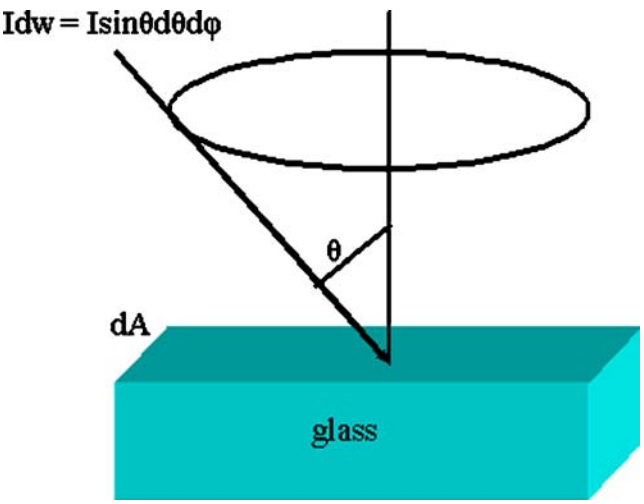

Fig. 1 Schematic representation of a beam incoming at a window with an angle of incidence θ

2.4.1 Shortwave radiation

The method used to compute the radiation reaching the indoor surface of the walls is similar to the one adopted in the UCP of Martilli et al. (2002). The solar energy penetrating through the windows is assumed to be uniformly distributed on the interior surfaces. Moreover, this radiation is reflected by the surfaces isotropically in all the directions.

The solar radiation captured by an indoor wall is the sum of the radiation coming directly from the windows and the radiation reflected by the other indoor walls. This shortwave radiation reaching a wall is indicated by Eqs. 13–15 (by "wall", here and in the rest of the article, we intend all the internal surfaces, including ceiling and pavement). For example, for the radiation reaching a wall i (more details on the symbols used in these equations are in the Appendix):

$$Rs_i = Rs + \sum_{j\neq i}\text{alb}_j Rs_j \psi_{ji} \qquad (13)$$

$$\psi_{ji} = \frac{A_j f_{ji}}{A_i} = f_{ij} \qquad (14)$$

$$\text{alb}_j = \text{alb}_{\text{wall},j}\left(1-\alpha_{\text{wind},j}\right) + \text{alb}_{\text{wind}} \times \alpha_{\text{wind},j} \qquad (15)$$

Equation 13 is a linear system of six equations and six unknowns (the radiation received by each wall) easy to solve by matrix inversion. The functions f_{ji} represent the view factors between wall j and wall i, and the term A_j is the area (m^2) of wall j. More details about the view factors can be found in Sparrow and Cess (1978).

2.4.2 Long-wave radiation

The long-wave radiation reaching an indoor wall i is the sum of the long-wave radiation emitted and reflected by the other walls. In order to compute the radiation, the following equations are used (more details on the symbols used in these equations are included in Appendix):

$$Rl_i = \sum_{j\neq i}\sigma\psi_{ji}\left(\widetilde{\varepsilon}_j T_{\text{wall},j}^4 + \widehat{\varepsilon}_j T_{\text{wind},j}^4\right) + \sum_{j\neq i}\left(1-\varepsilon_j\right) Rl_j \psi_{ji} \qquad (16)$$

$$\begin{aligned}\widetilde{\varepsilon}_j &= \varepsilon_{\text{wall},j}\left(1-\alpha_{\text{wind},j}\right)\\ \widehat{\varepsilon}_j &= \varepsilon_{\text{wind}}\alpha_{\text{wind},j}\\ \varepsilon_j &= \widetilde{\varepsilon}_j + \widehat{\varepsilon}_j.\end{aligned} \qquad (17)$$

This is, once again, a linear system of six equations and six unknowns easy to solve (the incoming long-wave and

short-wave radiation at the outdoor surfaces are coming from the mesoscale model).

2.5 Mathematical model of the air conditioning system

In BEM the indoor air temperature and humidity can be controlled with the help of the air conditioning system. We can decide when the air conditioning is working and when it is not. Kikegawa´s model (Kikegawa et al. 2003) is quite different because it supposes that the processed load H_{out} and E_{out} in Eqs. 3 and 4 are proportional to H_{in} and E_{in}, respectively ($H_{out}=\phi_p H_{in}$ and $E_{out}=\phi_p E_{in}$).

In our model the same method is used for the computation of H_{out} and E_{out}, and, hence, in the following only the computation of H_{out} will be explained. In the model the air conditioning system (here and in the following we use the term "air conditioning", even though heating can also be obtained with other systems) has a target temperature T_{target} and a gap of comfort ΔT fixed that the user can define.

If the air conditioning is not in use, then $H_{out}=0$. If it is, a first guess of the temperature at time $n+1$, called T^*, is computed as follows (it is the discretization of Eq. 1 by setting $H_{out}=0$),

$$T^* = \frac{\Delta t}{Q_B} H_{in}^n + T^n \tag{18}$$

At this point there are three possibilities:

(a) T^* lies within the comfort range, i.e. $|T^* - T_{target}| \leq \Delta T$, then $H_{out}{}^n=0$, and $T^{n+1}=T^*$.
(b) T^* is bigger than the target temperature plus the comfort range, i.e. $T^* > T_{target} + \Delta T$. In this case $H_{out}{}^n$ is calculated as:

$$H_{out}^n = H_{in}^n - \frac{Q_B}{\Delta t}\left(T_{target} + \Delta T - T^n\right) \tag{19}$$

However, if $\left|\frac{H_{out}^n - H_{in}^n}{Q_B}\right| > \delta$ (δ being the maximum power of cooling/heating (Ks^{-1}) of the air conditioning system, which is a fixed value dependent on the air conditioning system) Eq. 19 is not used and H_{out}^n is calculated as:

$$H_{out}^n = H_{in}^n + \delta Q_B \Rightarrow H_{in}^n - H_{out}^n = -\delta Q_B < 0. \tag{20}$$

Once $H_{out}{}^n$ is known, the temperature at time step $n+1$ is estimated as

$$T^{n+1} = \frac{\Delta t}{Q_B}\left(H_{in}^n - H_{out}^n\right) + T^n.$$

(c) T^* is smaller than the target temperature minus the comfort range, i.e. $T^* < T_{target} - \Delta T$. With a similar procedure to that of the previous paragraph,

$$H_{out}^n = H_{in}^n - \frac{Q_B}{\Delta t}\left(T_{target} - \Delta T - T^n\right) \tag{21}$$

If $\left|\frac{H_{out}^n - H_{in}^n}{Q_B}\right| > \delta$, Eq. 21 is not used, and $H_{out}{}^n$ is computed as:

$$H_{out}^n = H_{in}^n - \delta Q_B \Rightarrow H_{in}^n - H_{out}^n = \delta Q_B > 0 \tag{22}$$

and the temperature at time $n+1$ is $T^{n+1} = \frac{\Delta t}{Q_B}\left(H_{in}^n - H_{out}^n\right) + T^n$.

With this method, the indoor temperature always lies within a range of comfort (defined by the user), and the cooling/heating power will never be higher than a fixed value δ that depends on the properties of the air conditioning system. The same treatment is done with respect to the latent heat load E_{out}. Finally, we can calculate the total processed load $H_{out}+E_{out}$.

3 Verification of BEM (without the coupling with the UCP)

A combination of analytical, inter-program, and empirical testing procedure has been used for the verification and validation of the building energy model. The verification and the inter-program validation were made comparing the results of BEM against those obtained by Zmeureanu et al. (1987) with the models CBS-MASS, BLAST (BLAST-3.0, 1981), and TARP (Walton 1983). The simulations with BEM were done for a building with five floors. The results refer to the third floor (intermediate floor).

3.1 Verification

The verification is applied to a room 6.0×6.0×3.6 m^3 on the intermediate floor with four exterior walls and no windows. The indoor air is considered dry and the main assumptions are: no solar radiation, no sensible/latent heat generated by equipments and occupants, and constant long-wave radiation incoming at the exterior walls. More details about the inputs are presented in Table 1.

3.1.1 Variation of inside surface temperature of a wall due to a step change in outdoor air temperature

Initially, the temperature of the walls and room air are assumed to be 20°C. Then, while the room air temperature is kept constant at 20°C ($H_{in}=H_{out}$), the outdoor air temperature drops suddenly to 0°C ($\Delta T_0=20$°C). No air

Table 1 Physical parameters used for the simulation in the analytical validation

Parameters	Settings
Exterior walls	0.28 m brick
Intermediate walls (ceilings and floors)	0.28 m brick
Ground wall (Dirichlet b. c.)	0.28 m brick
Constant surface wall coefficient (indoor and outdoor)	8 WK^{-1} m^{-2}
Volumetric ventilation rate	3.6 m^3 m^{-2} h^{-1}
Physical properties used for brick	
Conductivity	0.73 WK^{-1} m^{-1}
Density	1.84×10^3 kg m^{-3}
Specific heat	900 J kg^{-1} K^{-1}
Emissivity	0.9

infiltration (β=1, in Eq. 3) is considered in this case. The temperature of the inside surface of the wall is analyzed and the comparison shows that results from BEM are in good agreement with analytical solutions and CBS-MASS (Fig. 2).

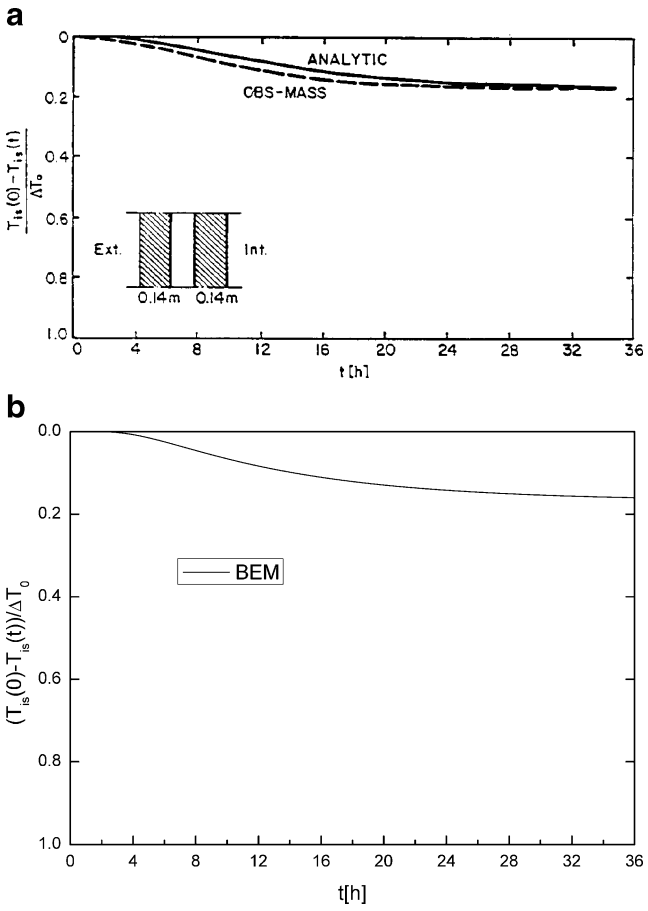

Fig. 2 Variation of the inside surface temperature for a 0.28 m deep brick wall due to a step change in outdoor air temperature: **a** analytical solution against CBS-MASS (From Zmeureanu et al. 1987); **b** variation obtained with BEM

3.1.2 Variation of room air temperature for a step change in outdoor air temperature

Initially, the temperature of the walls and room air are both equal to 20°C. The variation of the room air temperature, subject to a sudden drop of outdoor air temperature to 0°C (ΔT_0=20°C) is analyzed. The effect of air infiltration (β=0) and internal mass is studied. We impose that the temperature of internal mass (ceilings and floors on the intermediate floors) is constant and equal to their respective room air temperature ($T_{im}=T_R$) in the building. The results (Fig. 3) indicate good agreements between BEM, analytical solutions, and CBS-MASS. It is interesting to note that the evolution of the indoor air temperature is different on each floor (Fig. 4). On the top floor, the cooling of indoor air is faster than on the other floors because the roof is exposed to the cold outdoor air. In contrast, on the first floor the cooling is slower than on the other floors because we have imposed a net flux equal to zero at the lowest layer in the ground wall (Dirichlet boundary condition).

3.2 Inter-program validation

The inter-program validation deals with the comparison between the estimation of the space thermal loads provided by BEM against the predictions of three well-known programs in the thermal analysis of buildings: BLAST, TARP, and CBS-MASS. The comparison is performed in a winter design day (Table 2) for an intermediate floor office space 30×30×3.6 m^3, with four exterior walls and windows. The main characteristics used in this space are presented in Table 3. It is important to point out that in our simulation the solar radiation incoming at each intermediate floor is the same. In this test BEM was not linked to the UCP (Martilli et al. 2002) because, if it was, distinct floors would receive different radiation fluxes due to shadowing effects induced by neighboring buildings. For this reason the results of an intermediate floor in the test are almost

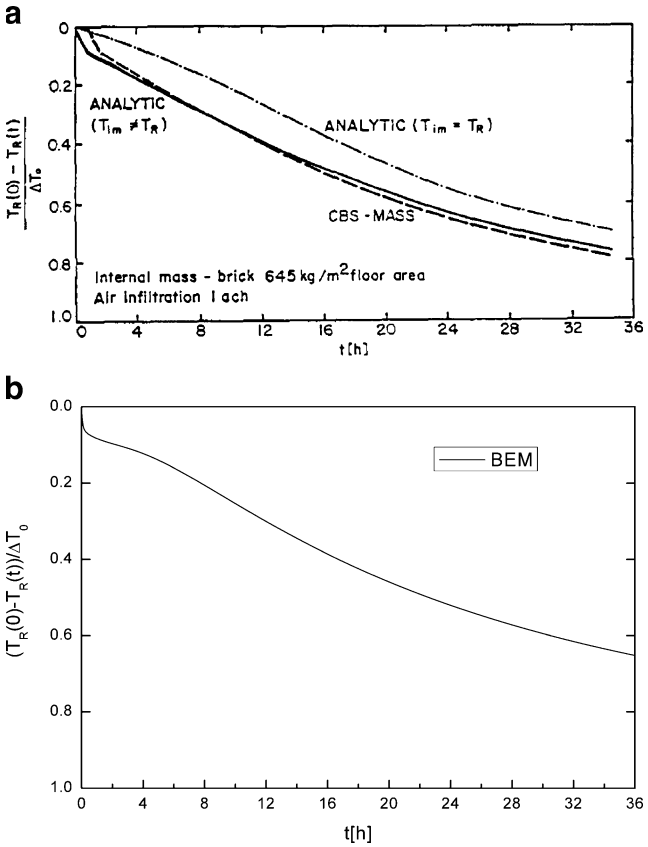

Fig. 3 Variation of the room air temperature due to step change in outdoor air temperature (internal mass and air infiltration are considered): **a** analytical solution against CBS-MASS (From Zmeureanu et al. 1987); **b** variation obtained with BEM

Table 2 Weather data for the inter-program validation in a winter design day

Hour (h)	Outdoor temperature (ºC)	Direct normal radiation (Wm^{-2})
1	−18.05	–
2	−18.80	–
3	−19.40	–
4	−19.85	–
5	−20.00	–
6	−19.70	–
7	−18.95	–
8	−17.60	–
9	−15.65	398.1
10	−13.40	685.9
11	−10.85	794.5
12	−8.45	833.7
13	−6.65	830.0
14	−5.45	781.2
15	−5.00	652.7
16	−5.45	301.9
17	−6.50	–
18	−8.15	–
19	−10.10	–
20	−12.05	–
21	−13.70	–
22	−15.20	–
23	−16.40	–
24	−17.30	–

independent of the height of the building. Thus, the largest differences only occur between the top or the ground floor and the intermediate floors. The top floor exchanges more energy (solar radiation and heat conduction through its roof) than the other floors. On the other hand, on the first floor the flux exchanged through the ground (generally in contact with the soil) is different when compared against the intermediate floors. Figure 5 shows the results of the space thermal load ($-H_{out}$) necessary to maintain the indoor air temperature constant (20ºC in this case) as estimated by the BLAST, TARP, and CBS-MASS programs against BEM. Dry air was considered ($E_{in}=E_{out}=0$) in the simulation. The comparisons show that BEM provides estimations of the heating load close to those of the other models. The small differences observed may also be a consequence of the uncertainties on the values of some parameters (incoming long-wave radiation at the outdoor surfaces and convective heat transfer coefficient at the exterior wall) that were not explicitly mentioned in Zmeureanu et al. (1987). Moreover, the radiation reflected by the ground and other buildings, and incoming at the exterior walls, is not considered in BEM and it is not clear if it was taken into account by Zmeureanu et al. (1987).

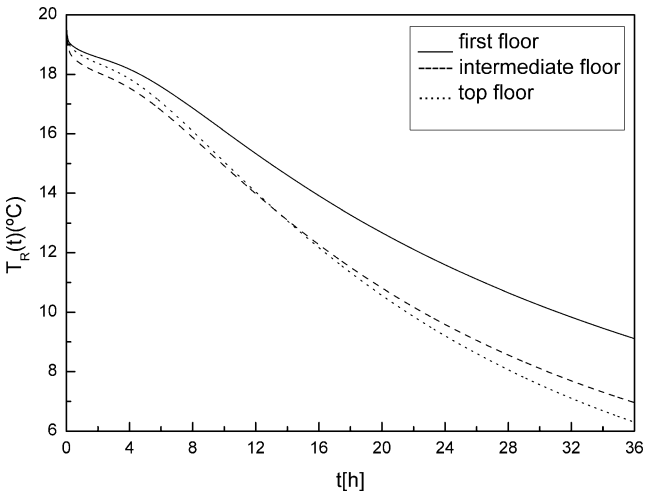

Fig. 4 Variation of the room air temperature in different floors obtained with BEM (as in Fig. 3)

Table 3 Physical parameters used for the simulation in the inter-program validation

Parameters	Settings
Exterior walls	0.10 m concrete
	0.10 m insulator
	0.02 m gypsum board
Intermediate walls (ceilings and floors)	0.10 m concrete
	0.10 m insulator
	0.02 m gypsum board
Ground wall (Dirichlet b. c.)	0.22 m concrete
Constant surface wall coefficient (indoor and outdoor)	8 $WK^{-1} m^{-2}$
Constant surface window coefficient (indoor and outdoor)	2.8 $WK^{-1} m^{-2}$
Air infiltration	β=0
Volumetric ventilation rate	3.6 $m^3 m^{-2} h$
Glazing-to-wall ratio (double standard glazing)	0.5
Internal heat gains	30 Wm^{-2} between the 9:00 to 17:00
Room air temperature	20°C
Physical properties used for the materials	
Emissivity	0.9
Concrete	
Conductivity	1.73 $WK^{-1} m^{-1}$
Density	2.35×10^3 kg m^{-3}
Specific heat	880 J $kg^{-1} K^{-1}$
Albedo	0.2
Insulator	
Conductivity	0.057 $WK^{-1} m^{-1}$
Density	13 kg m^{-3}
Specific heat	840 J $kg^{-1} K^{-1}$
Gypsum board	
Conductivity	0.14 $WK^{-1} m^{-1}$
Density	760 kg m^{-3}
Specific heat	800 J $kg^{-1} K^{-1}$
Albedo	0.7

3.3 Comparison of BEM against other box model to validate the air conditioning system

This last validation deals with the comparison between BEM and the model of Kikegawa et al. (2003) using data collected in a campaign over Tokyo (Japan). The measurement data were acquired in August, 1998 for a 25-story office building (building-O) located at the center of a business area (Ootemachi). The measurement includes the continuous acquisition of meteorological data, Fig. 6, from the rooftop of the building of approximately 100 m height. The simulation was initialized at 0000 LST, 2 August and terminated at 2400 LST, 5 August 1998. The simulations started on a Sunday, during the Pacific Ocean anticyclone and under typical summer-day conditions. In our validation of the air conditioning system we have compared the total processed loads ($H_{out}+E_{out}$) for the building-O (the dimensions considered in each floor were$47.0\times47.0\times3.78$ m^3) obtained by BEM with the one generated by Kikegawa´s model. Even though the calculation of the processed load is rather different in the two models, the results are quite similar (Fig. 8). Hence, it is possible to say that BEM is capable of capturing the most important mechanisms governing heat generation within buildings and exchanges with the exterior. While comparing the two models, we forced the exterior meteorological variables (temperature and humidity) to the measured values. The aim of this test was the validation of the air conditioning model, and not

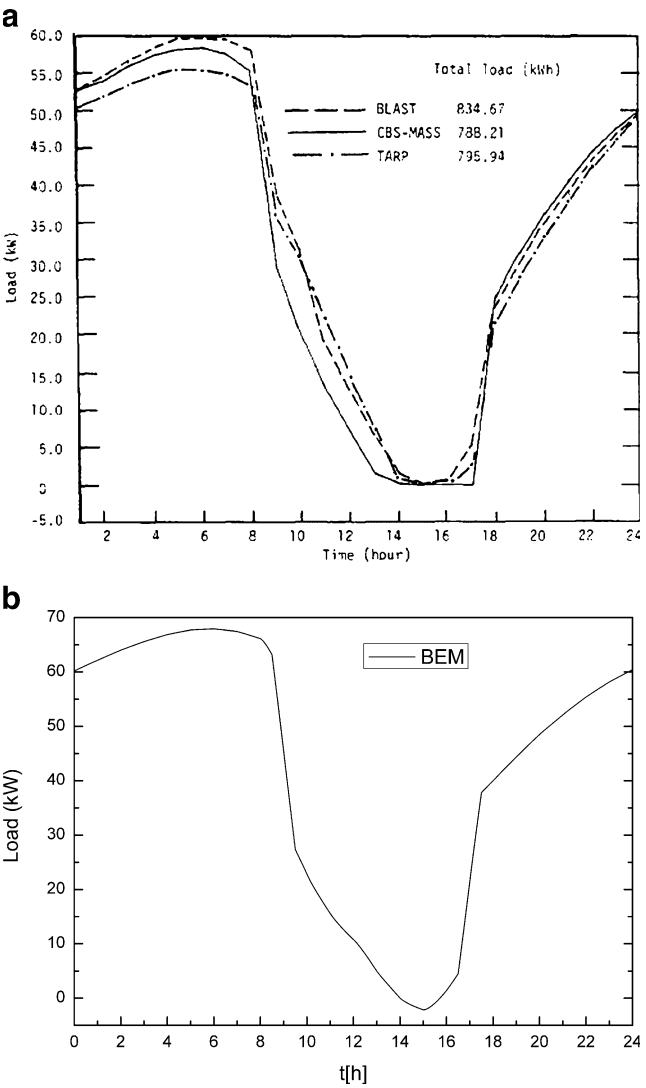

Fig. 5 Comparison of the thermal load for an office space on a winter design day in an intermediate floor: **a** estimations of CBS-MASS, BLAST, and TARP (From Zmeureanu et al. 1987); **b** estimations obtained with BEM

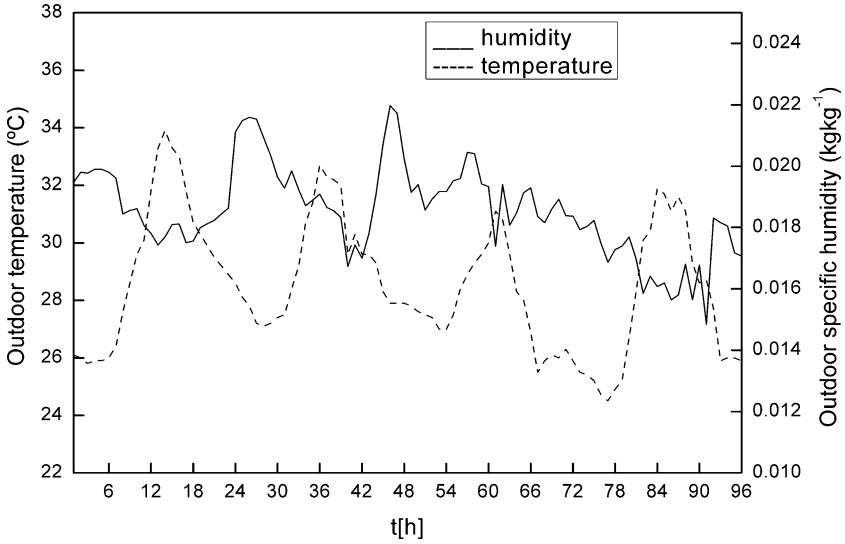

Fig. 6 Temporal series of the outdoor temperature (*left*) and specific humidity (*right*) used in the period of simulation and measured at the top of the building-O

the study of the interactions between BEM and the atmosphere.

Temporal variations of ϕ_p and q_E in Eq. 3 used in the simulation are shown in Fig. 7. The parameters of typical office buildings were adopted (Table 4) for the structures and the air conditioning systems. In Fig. 8 one can see the total (sensible and latent) cooling energy for the building-O (obtained adding up over every level, 25 floors) computed with BEM and Kikegawa´s model. Observe that the BEM's air conditioning model is able to reproduce results similar to those obtained by Kikegawa.

4 Sensitivity of the processed load to different physical processes

As explained, the air temperature and humidity inside a building, and the energy needed to control them (through air conditioning or heating), are influenced by several physical processes (the different terms on the right-hand sides in Eqs. 3 and 4). In this section, we present a series of simulations with the goal of analyzing the sensitivity of the processed load (e. g. the energy needed to control air temperature and humidity) to these different processes.

The simulations were performed fixing $H_{out}=H_{in}$ for each floor. The following results (Fig. 9) are obtained by adding the total load of the different floors. The same building parameters and conditions used in Section 3.2 were considered. In the following, by "base case" simulation we will refer to the one described in Section 3.2.

The first test deals with the impact of the radiation through the windows. Two simulations were performed, by modifying the base case: one simulation without windows ("no window" case), where no radiation is entering the building ($\alpha_{wind,j}=0$, in Eq. 15), and the other one with the internal albedo of the windows equal to 1, once the

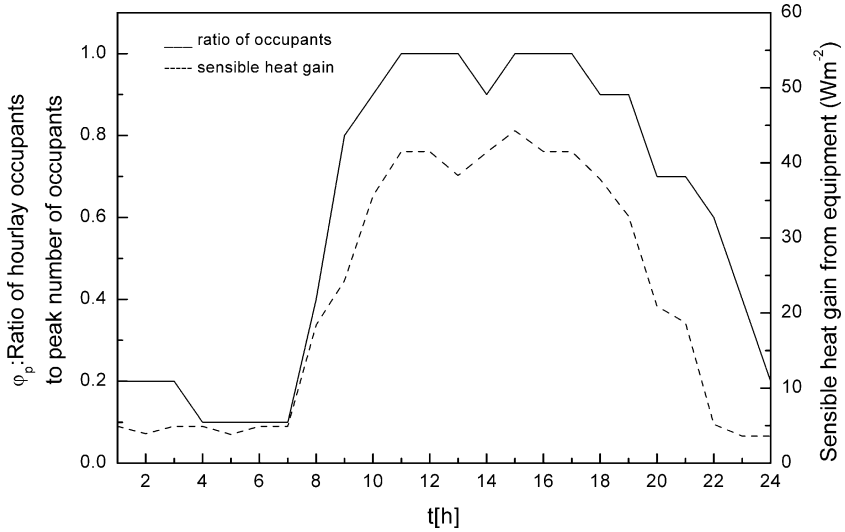

Fig. 7 Time-dependent parameters ϕ_p (*right*) and q_E (left) used in weekdays

Table 4 Parameters used in the validation of BEM against Kikegawa´s model

Parameters	Settings
Exterior vertical walls	0.11 m concrete
	0.05 m insulator
	0.11 m concrete
Intermediate walls (ceilings and floors)	0.22 m concrete
Ground wall (Dirichlet b. c.)	0.33 m concrete
	1.07 m soil
Constant surface wall coefficient (indoor and outdoor)	8 $WK^{-1}\ m^{-2}$
Constant surface window coefficient (indoor and outdoor)	2.8 $WK^{-1}\ m^{-2}$
Duration of air conditioning on weekdays	0900-1900 LST[a]
Target temperature of room cooling	26.0ºC
Target relative humidity of room cooling	50.0%
Volumetric ventilation rate per unit floor area	5.0 $m^3\ m^{-2}\ h^{-1}$
Thermal efficiency of the total heat exchanger (β)	60%
Floor area per occupant	5 m^2/person
Sensible heat generation from an occupant (q_{hs})	54.7 W/person
Latent heat generation from an occupant (q_{hl})	64.0 W/person
Insolation transmittance through the windows (windows with blinds)	30%
Glazing-to-wall ratio	30%
Parameters own of BEM	
Comfort range of temperature	0.1 K
Power of cooling/heating	10^{-3} K s^{-1}
Comfort range of humidity	10^{-3} kg kg^{-1}
Power of drying/moistening	10^{-6} (kg kg^{-1})s^{-1}
Physical properties used for the materials	
Emissivity	0.9
Concrete	
Conductivity	1.39 $WK^{-1}\ m^{-1}$
Volumetric heat capacity	1.93 10^6 J m^{-3} K^{-1}
Albedo	0.2
Insulator	
Conductivity	0.04 $WK^{-1}\ m^{-1}$
Volumetric heat capacity	0.06×10^6 J m^{-3} K^{-1}
Soil	
Conductivity	1.00 $WK^{-1}\ m^{-1}$
Volumetric heat capacity	1.74×10^6 J m^{-3} K^{-1}

[a] Pre-cooling starts from 0800 LST

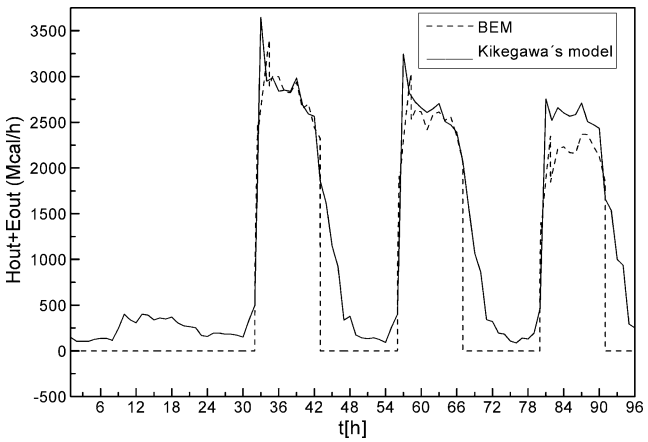

Fig. 8 Comparison of the total processed load in building-O obtained with BEM and with the Kikegawa´s model

radiation is inside the floor ("total trapping" case). The aim of this second case is to simulate the impact of the internal walls in the building (rooms) that may prevent the radiation from exiting windows, and trap the totality of the solar radiation entering the building. The results (Fig. 9a) show that in this winter case, the absence of windows reduces the energy consumption during the night. The reason is that the glasses have a higher heat capacity than the walls and the heat flux exchanged with the air is smaller than the flux exchanged through the walls. In contrast, during the day, the absence of windows increases the energy consumption because there is no radiation penetrating the floor and it is more difficult to maintain a warm indoor temperature. The effect due to considering indoor walls in a floor (total trapping) is small and the decision not to account for them is justified.

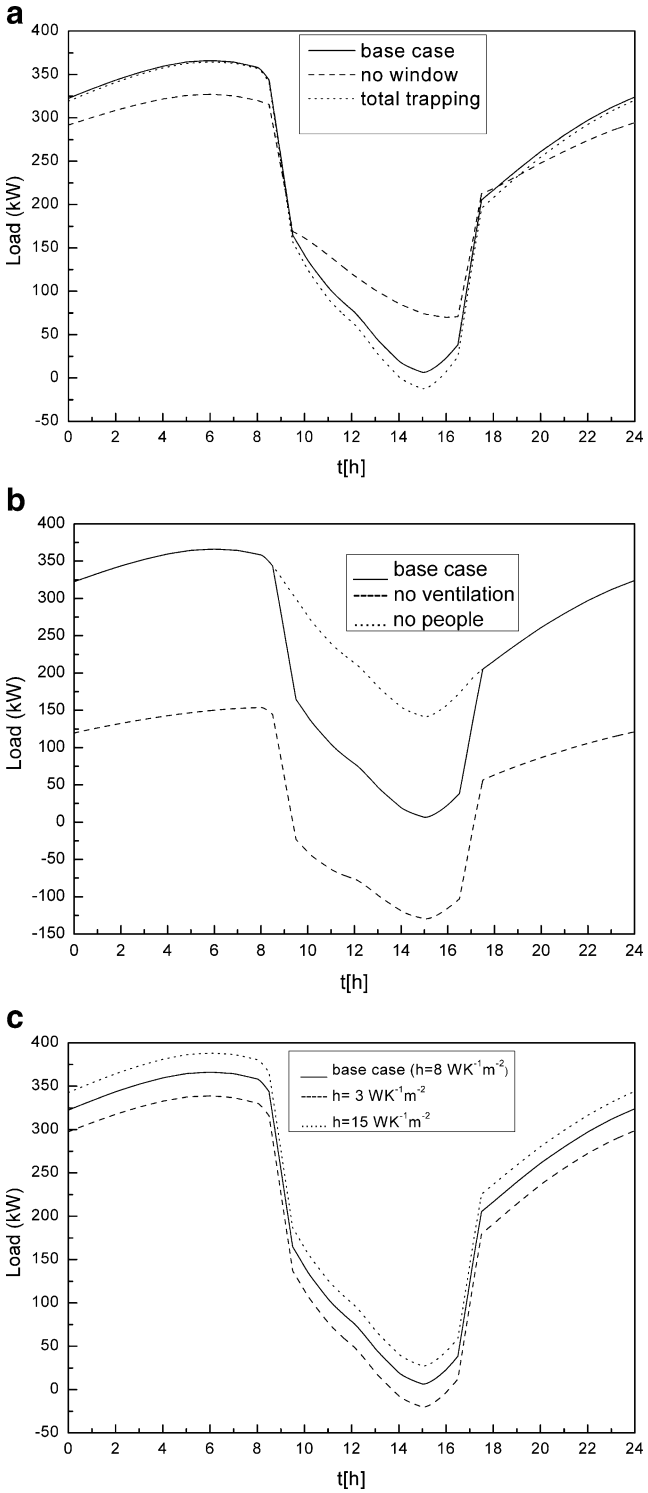

Fig. 9 Estimations of the total thermal load for the office building in different situations: **a** comparison to study the impact of the radiation through the windows; **b** comparison to study the impact of the natural ventilation and the heat released by people and equipments; **c** comparison to study the impact of the convective heat transfer coefficients

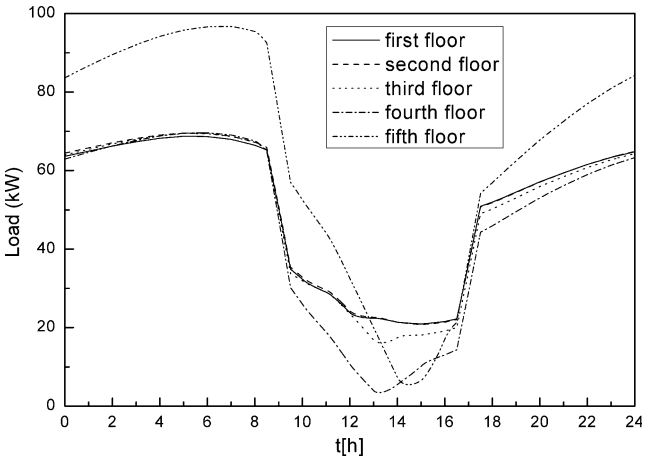

Fig. 10 Comparison of the thermal load over various floors in an office building when the incoming radiation is different for each floor

The second test (Fig. 9b) was performed to investigate the impact of natural ventilation and the heat released by people and equipments. One simulation was done without people or equipments ("no people" case, $\phi_p=0$ and $q_E=0$ in Eq. 3), and another with no ventilation ("no ventilation" case, $\beta=1$ in Eq. 3). For this winter simulation, the impact of people and equipments is of about 150 kW during daytime (during night time people were absent also in the base case). It is also interesting to notice the importance of ventilation: for this winter case, during the night, the lack of ventilation results in a decrease in energy consumption, while during daytime, energy is required to cool down the air in the building[2] heated up by the radiation, and internal sources (people and equipments).

The third test (Fig. 9c) was carried out to study the effect of the convective heat coefficients at the external surfaces.[3] Usually, these coefficients are estimated as a function of wind speed. However, there is still a significant uncertainty in the determination of such a relationship (see Martilli et al. 2002, Masson 2000). One simulation was carried out with a value smaller (3 WK^{-1} m^{-2}) than in the base case (8 WK^{-1} m^{-2}) and another with a higher value (15 WK^{-1} m^{-2}). As one can observe in the graph, the processed loads are sensitive to these coefficients, with a maximum variability of about 50 kW.

[2] It must be remembered here that the ventilation has an impact not only on air temperature, but also on indoor air quality (for example, it helps to disperse pollutants emitted indoor). The optimal ventilation must then, takes into account both effects.

[3] The convective heat coefficient h is used to estimate the sensible heat H exchanged between the external wall surface and the atmosphere, using the formula $H=h\ (T_a-T_{wall})$, where T_{wall} is the temperature of the external surface of the wall, and T_a is the outdoor air temperature. H enters in the surface energy budget at the external surface and gives the b.c. for the heat diffusion equation in the wall.

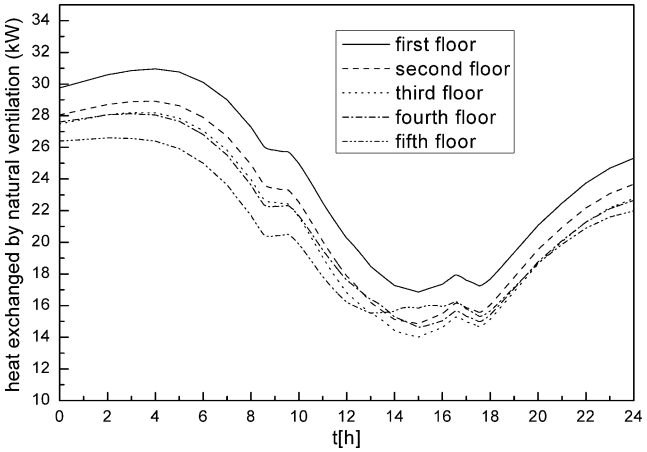

Fig. 11 Comparison of the heat exchanged through natural ventilation for the office building over different floors (no regulation of the indoor air temperature)

Finally, a simulation with a different outdoor input radiation for every floor was conducted. A five floor building (15 m high, with floors 3 m high), in a street 15 m wide, (H/W=1) was considered to compute the outdoor radiation. Using the parameterization of Martilli et al. (2002), the solar radiation reaching the walls (accounting for shadowing and reflections) was computed for every floor and for a N–S and W–E street orientation. Four radiations (for North, South, West, and East walls) were obtained for each floor. Such values were then used as an input to BEM to compute the processed load in the same conditions than in the base case. As one can see in Fig. 10, when the incoming radiation fluxes are different in every level, the load is different for every floor. In particular, the fifth floor loses more energy during night time and needs more energy to keep the temperature constant. On the other hand, during daytime, the upper floors receive more solar radiation (less shadowing) than the lower floors and need less energy to keep the temperature constant (for this winter case).

The last test was performed with the same configuration, but without any control over the indoor temperature H_{out}= 0. The temperature of the different floors could fluctuate freely in response to the different forcings. This affects the exchanges of heat between the indoor and outdoor air through ventilation. In fact, as shown in Fig. 11, having different temperatures on each floor, the heat fluxes due to ventilation are also different.

These last two examples show that it is important to consider the presence of floors in the building in the estimation of energy consumption, as well as in the calculation of the heat exchanged between the indoor and the outdoor air.

5 First results about the impact of BEM in the UCP

In this last section, we present preliminary results about the impact of BEM in the UCP of Martilli. The UCP-BEM scheme has been coupled to the mesoscale model FVM (Clappier et al. 1996) and simulations in a vertical column (neglecting horizontal derivatives) have been carried out in an ideal middle latitude city in a summer day. The ideal city is composed of cubical buildings 15 m high (H/W=1). To study the feedback between the air conditioning systems and the atmosphere, two different simulations were carried out using the same building parameters. In the first simulation, the heat extracted by the air conditioning systems is directly released into the atmosphere, while in the second it is not (i.e., the feedback between the building

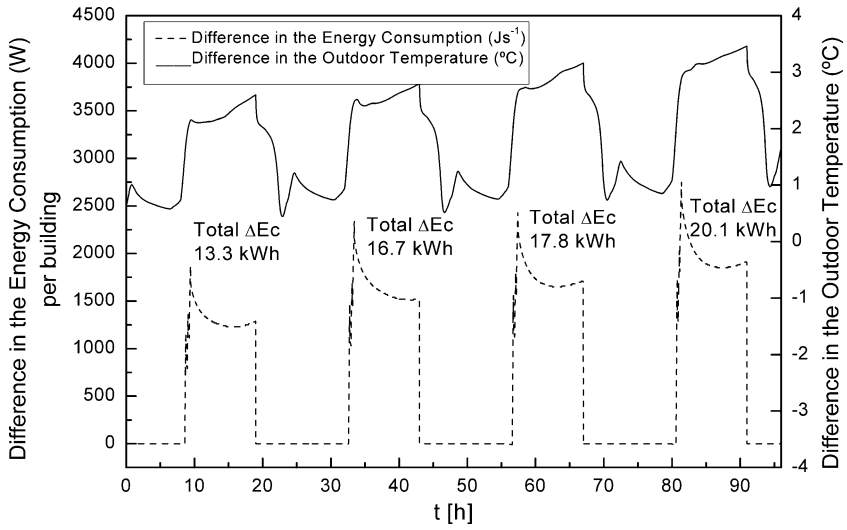

Fig. 12 Comparison of the difference in the energy consumption and the outdoor temperature for 4 days of simulations. In the first case the heat is released directly into the atmosphere and in the second one the heat is released into a sewage or in the soil

with the air conditioning and the atmosphere is not taken into account). Both simulations were carried out without considering people or equipments (φ_p=0 and q_E=0 in Eq. 3), with 30% of windows and without any natural ventilation (β=1 in Eq. 3). Standard values of the air conditioning system (the air conditioning was working from 8:00 to 19:00 every day, and the target temperature was 25ºC) and building materials were used. In Fig. 12, one can observe the temporal evolution of the difference in the air temperature on top of the buildings (where heat is released) between the two simulations ΔT (°C) during a 4-day period. Moreover, the temporal evolution of the difference in energy consumption (W), as well as the total daily variation in energy consumption ΔE_C (kWh) (here 1 kWh=3.6×10^6 J) per building, have been computed. The results show that when the air conditioning is working, the heat released into the atmosphere can increase the outdoor air temperature by 2 to 3°C. It is important to mention that when the outdoor air temperature increases, the energy necessary to maintain the indoor temperature within the comfort range also increases. Even though the results are not conclusive in these simulations (the atmospheric heating may be overestimated because the horizontal advection is not accounted for), one can clearly see that the impact of the air conditioning systems on the urban atmosphere is not negligible. Finally, the relative difference ($\Delta E_c/E_c$) has been computed to evaluate the feedback effects. In our 4-day simulation, the corresponding values were 6.33%, 7.88%, 8.42%, and 9.53%, respectively. The results indicate that an increase in air temperature of about 2°C corresponds to an increment in energy consumption of approximately 7–8%.

6 Conclusions

The verification indicates that BEM has accurately simulated the basic heat transfer phenomenon. The inter-program validation provides important information about the accuracy of BEM compared with other well-known computer programs used in the thermal analysis of buildings. These results show that BEM is able to capture the most important mechanisms governing heat generation within buildings and exchanges with the exterior. It is simpler and less CPU expensive than other building energy models and can be easily coupled with an UCP for mesoscale models. Moreover, BEM is able to reproduce the effects of the air conditioning systems. Finally, the sensitivity test (Section 4) shows the importance of considering different floors. A more detailed validation of BEM in the UCP of Martilli is carried out in Part II of this work (Salamanca and Martilli 2009), using meteorological data recorded during the BUBBLE campaign over Basel (Switzerland).

In conclusion, this work is a first step towards a modeling tool that can account for the complex interactions between urban climate, air pollutant dispersion, and the energy demand of buildings. Such a tool can be an important support to urban planners.

Acknowledgements The authors wish to thank CIEMAT and LPAS-EPFL for the doctoral fellowships held by Francisco Salamanca and Andrea Krpo, respectively. We also thank Y. Kikegawa for providing important data for the validation. This work has been funded by the Ministry of Environment of Spain.

Appendix

List of symbols

$\mathrm{alb}_{\mathrm{wall},j}$	albedo of the indoor surface of the wall j
A_f	floor area (m^2)
A_i^{wall}	surface area of the wall i (m^2)
A_j^{wind}	surface area of window in the wall j (m^2)
C_p	specific heat of air (J K^{-1} kg^{-1})
$h_{\mathrm{wall},i}$	convective heat transfer coefficient between the indoor air and the wall i (WK^{-1} m^{-2})
$h_{\mathrm{wind},j}$	convective heat transfer coefficient between the indoor air and the window in the wall j (WK^{-1} m^{-2})
l	latent heat of evaporation (J kg^{-1})
T_a	outdoor air temperature (K)
T_r	indoor air temperature (K)
$T_{\mathrm{wall},i}$	indoor surface temperature of the wall i (K)
$T_{\mathrm{wind},j}$	temperature of the window in the wall j (K)
P	peak number of occupants per floor area (person m^{-2})
q_E	sensible heat gain from equipments per floor area (W m^{-2})
q_{hl}	latent heat generation from the occupants (W $person^{-1}$)
q_{hs}	sensible heat generation from the occupants (W $person^{-1}$)
q_{Va}	specific humidity of the outdoor air (kg kg^{-1})
q_{Vr}	specific humidity of the indoor air (kg kg^{-1})
Rl_j	total long-wave radiation flux received by the wall j (W m^{-2})
Rs	solar radiation energy crossing the windows received directly by the indoor walls (W m^{-2})
Rs_j	total shortwave radiation flux received by the wall j (W m^{-2})
V_a	total ventilation rate (m^3 s^{-1})
$\alpha_{\mathrm{wind},j}$	% of window in the wall j
β	thermal efficiency of the total heat exchanger, $0 \le \beta \le 1$
$\varepsilon_{\mathrm{wall},j}$	emissivity of the indoor surface of the wall j
$\varepsilon_{\mathrm{wind}}$	emissivity of the windows

φ_P ratio of hourly occupants to P, $0 \leq \varphi_p \leq 1$
ρ air density (kg m^{-3})
σ Stefan-Boltzmann constant (W m^{-2} K^{-4})

References

BLAST-3.0-1981. The Building Loads Analysis and System Thermodynamics Program, Users Manual, U. S. Army Construction Engineering Research Laboratory, Champaign, Illinois, March.

Clappier, A., Perrochet, P., Martilli, A., Muller, F. and Krueger, B. C. 1996. A new nonhydrostatic mesoscale model using a CVFE (control volume finite element) discretisation technique, in P. M. Borell et al (eds.), Proceedings, EUROTRAC Symposium '96, Computational Mechanics Publications, Southampton, pp. 527–531

Karlsson J, Roos A (2000) Modelling the angular behaviour of the total solar energy transmittance of windows. Sol Energy 69:321–329

Kikegawa Y, Genchi Y, Yoshikado H, Kondo H (2003) Development of a numerical simulation system toward comprehensive assessments of urban warming countermeasures including their impacts upon the urban buildings energy-demands. Appl Energy 76:449–466

Kusaka H, Kondo H, Kikegawa Y, Kimura F (2001) A simple single-layer urban canopy model for atmospheric models: comparison with multi-layer and slab models. Bound-Lay Meteorol 101:329–358

Martilli A, Clappier A, Rotach MW (2002) An urban surface exchange parameterization for mesoscale models. Bound-Lay Meteorol 104:261–304

Masson V (2000) A physically based scheme for the urban energy budget in atmospheric models. Bound-Lay Meteorol 94:357–397

Oke, T. R. 1987, The surface energy budget of urban areas, in Modeling the Urban Boundary Layer, edited by the American Meteorological Society, 1–52.

Roos A (1997) Optical characterisation of coated glazings at oblique angles of incidence: measurements versus model calculations. J Non-Cryst Solids 218:247–255

Salamanca F, Martilli A (2009) A new building energy model coupled with an urban canopy parameterization for urban climate simulations—Part II. Validation with one dimension off-line simulations. Theor Appl, Climatol. doi:10.1007/s00704-009-0143-8

Sparrow EM, Cess RD (1978) Radiation Heat Transfer. Brooks/Cole, Belmont, p 366

Walton, G. N. 1983. Thermal Analysis Research Program (TARP) Reference Manual, U. S. Department of Commerce, National Bureau of Standards, National Engineering Laboratory, Washington, DC, March.

Zmeureanu R, Fazio P, Haghighat F (1987) Analytical and interprogam validation of a building thermal model. Energy Build 10:121–133